AMERICAN
METEOROLOGICAL
SOCIETY

Journal of Climate

EARLY ONLINE RELEASE

This is a preliminary PDF of the author-produced manuscript that has been peer-reviewed and accepted for publication. Since it is being posted so soon after acceptance, it has not yet been copyedited, formatted, or processed by AMS Publications. This preliminary version of the manuscript may be downloaded, distributed, and cited, but please be aware that there will be visual differences and possibly some content differences between this version and the final published version.

The DOI for this manuscript is doi: 10.1175/2010JCLI3232.1

The final published version of this manuscript will replace the preliminary version at the above DOI once it is available.

Solar Cycles in 150 Years of Global Sea-Surface Temperature Data

By Jiansong Zhou and Ka Kit Tung

Department of Applied Mathematics

University of Washington

Seattle, Washington, USA

(Corresponding author: K. K. Tung: tung@amath.washington.edu)

Abstract

The purpose of the present work is to demonstrate that a solar-cycle response exists in surface temperature using the longest global dataset available, which is in the form of Sea-Surface Temperature (SST) 1854-2007, with emphasis on methods and procedures, data quality and statistical tests, and the removal of deterministic signals such as volcano aerosol forcing and greenhouse gas warming. It is found, using the method of Composite-Mean Difference (CMD) Projection, a signal of warming during solar max and cooling during solar min years in the global SST over the 14 cycles, dispelling previous claims that the solar-cycle response is opposite before 1920 as compared to the modern era. The magnitude of the solar cycle response averaged over the oceans between 60S and 60N is about 0.1 C per Wm^{-2} of variation of the solar constant (but is slightly lower, at ~0.085 C, when periods of suspected bad data are averaged in, consistent with the previous results of White *et al.* [1997]). The signal is robust provided that we exclude the years near the Second World War; during which transitions from British ships to US ships introduced warm bias in the SST, as discovered by Thompson *et al.* [2008] . Monte-Carlo tests show that the extracted signal has less than 0.02% chance of being a random occurrence. This establishes the existence of a solar-cycle response at the earth's surface at high statistical confidence. Contamination of the signal by volcano aerosols is estimated using the Multiple CMD Inversion method and found to be small over this long record, although ENSO contamination varies depending on the period chosen but is also small.

The multi-decadal trend of response to solar forcing is found to account for no more than a quarter of the observed warming in SST during the past 150 years, under a reasonable but unproven assumption that the climate response to secular solar forcing and to solar cycle forcing has the same spatial pattern.

1. Introduction

The Sun's radiant output varies quasi-periodically on a 10-11 year timescale. In its active phase, called the solar max, the Sun has more dark sunspots and accompanying bright faculae. The magnitude and indeed even the sign of this variation on the solar constant (the Total Solar Irradiance (TSI)) were uncertain until the advent of satellites in 1979, when direct measurement above the earth's atmosphere became feasible. Using sunspot and other proxy indices, the variation of the TSI can be extended using solar models back to the 17th century. The controversy concerning the TSI reconstruction is related to the secular trend of the TSI and generally is not on the classification of whether a year belongs to solar max or solar min (see e.g. Scafetta and Willson [2009]). Only this latter minimal information is used in the present work. The terrestrial response to this variable forcing is more controversial, especially with regards to the temperature at the surface. Historically there were debates as to whether the Earth was warmer or colder during the solar max as compared to the solar min. Although we previously found using modern temperature records that the global-mean temperature is warmer during solar max, there were controversial reports that perhaps in an earlier epoch the response was opposite. For example, the literature reviewed by Hoyt and Schatten [1997] , Chapter 5, suggests that the surface temperature is negatively correlated with the TSI during the period 1800-1920, and positively correlated from 1920 to present, and a sign reversal was observed in the apparent dependence of water levels in Lake Victoria around 1920 (Clayton [1940]). This phase reversal, if true, is difficult to understand from physical reasoning and makes the search for the mechanism of the solar cycle response more elusive. One possibility could be that our Sun is at the borderline between overcompensation and under-compensation of the dimming effect of the sunspots by the brightening effect of the faculae. However, modern reconstructions of the TSI, e.g. Lean [2005]; Lean and Rind [1998]; Lean *et al.* [1995] , do not show this reversal between TSI maximum and sunspot number maximum.

When dealing with historical data, a major problem is that of data quality, especially during periods of world wars. Camp and Tung [2007a] and Tung and Camp [2008] found a statistically significant global temperature warming at the surface (land plus ocean) during solar max in two reanalysis datasets since late 1950s, by which time some of the data problems likely have been corrected. Tung *et al.* [2008] additionally found similar response in the two *in situ* data records, during the same period. Questions remain concerning the existence of the solar-cycle response at the surface in earlier decades and in century-long records. A simple extension of our previous work, which was done for the period from 1950s on, to earlier periods immediately runs into the period of World War II, when the data was problematic, as pointed out recently by Thompson *et al.* [2008] .

Although "global" surface temperature datasets are available that start from 1880, large continental areas have missing coverage, with the exception of parts of North America, Europe and Japan. Some datasets fill in the missing data using various methods, as reviewed in Tung *et al.* [2008]. Generally, the solar-cycle signal obtained by composite-mean difference is smaller in areas where the missing data were filled in, as these various interpolation schemes tend to reduce the anomaly to varying degree. Recent satellite data (used in reanalysis) shows that larger responses tend to occur over continents relative to the oceans and they are larger over the Arctic and Antarctic relative to the tropics. Since these higher response regions are the ones more likely to have experienced severe missing data in the long-term record, it is expected that the global mean signal in the long-term historical record with missing data is smaller than what could have been found in geographically complete data record.

A related issue on the existence of the solar-cycle response is the fact that there were major volcano eruptions that happened to be spaced on a decadal scale during the recent period: Agung in 1963, El Chichon in 1982 and Pinatubo in 1991. Previously, using 100 years of surface temperature data and optimal filters constructed using a two-dimensional energy balance model, North and Stevens [1998] found that the volcano signal contributed significantly to the decadal peak in the climate signal spectrum. Such contaminations prevented the authors from detecting the solar signal with confidence, in contrast to their earlier work (Stevens and North [1996]), where a "fairly robust solar signal" was found when other deterministic climate signals (such as volcano eruptions and anthropogenic warming) were ignored. Lean and Rind [2008]) recently also pointed out that such volcano contamination could affect methods such as Fourier analysis, which is global in time. It should in principle not affect as much the local-in-time methods such as those used by us (Camp and Tung [2007a]; Tung and Camp [2008]; Tung *et al.* [2008]). We, in our previous work, additionally removed two years after the major eruptions, when significant aerosol induced cooling were observed. Nevertheless it would be reassuring if the solar signal can still be found during periods when the stratosphere was clear of volcano aerosols, or when the period studied is long enough that the time of occurrence of major volcanoes can be taken as random and averaged out when we take the composite means of solar max and solar min and then difference them. A long data record affords us both possibilities. In addition, we will present an analysis using a novel method, which we called Multi-CMD Inversion method, to show that volcano and ENSO contaminations are small in our solar results.

Previously there are a number of important papers in the oceanographic literature dealing with the upper oceans' response to the radiative forcing from the Sun. Of these the work of White *et al.* [1997] stood out. They pointed out that since almost 90% of the change in TSI on decadal and interdecadal timescales is at wavelengths that penetrate to the troposphere, it is plausible that direct radiative forcing by the changing solar insolation of the upper ocean can give rise to a solar signal in the SST. Using 92 years of the Global Ice and Sea Surface Temperature (GISST) data from 1900-1991, White *et al.* [1997] obtained a band-passed decadal signal with an amplitude of 0.08±0.01 C per Wm^{-2} of the TSI in the globally averaged (from 40 S to 60 N) SST. The methods used were Cross Spectrum and Singular Spectrum Analyses. The peaks of the SST appear to approximately align with the peaks of the TSI except during the beginning of the century and during 1940s and early 1950s; they suspected that the latter discrepancy occurs because of the disruption in the collection of marine data during the WW II, which turned out to be the case. Allen [2000] applied the multi-taper frequency-domain singular value decomposition method to the Hadley Center global surface temperature record from 1871-1994, and found a strong spectral peak in the 10-13 year period, which he called the Quasi-Decadal Oscillation (QDO). A visual inspection of the time series of this QDO now shows coherence with the 11-year solar TSI variation, although no correlative study was done by the author. Nevertheless it appears that an 11-year solar signal in global surface temperature exists in Allen's filtered data. White and Tourre [2003] similarly found a statistically significant QDO peak in the 93 year (1900-1992) SST spectrum, as did Tourre *et al.* [2001] earlier in the 92 year (1900-1991) SST spectrum, and commented that the time series of the QDO appear to align with the solar irradiance variation. These methods are all of the Fourier type, and may be subject to the volcano contamination mentioned above. We hope our work will be able to directly address the contamination due to volcano and other deterministic signals, such as greenhouse gas warming and ENSO. A new method is introduced in section 9 to separate out these various other contributions.

2. Data

Currently the longest homogeneous instrumented record of surface temperature exists in the Sea-Surface Temperature (SST), which spans 150 years from 1854 to 2007, in the form of Extended Reconstructed Sea-Surface Temperature (ERSST) (*NOAA_ERSST_V3* data provided by the NOAA/OAR/ESRL PSD, Boulder, Colorado, USA, from their site at http://www.cdc.noaa.gov/*)*, as described in Smith and Reynolds [2003]; Smith and Reynolds [2004]; Smith *et al.* [2008] . The dataset was based on the Comprehensive Ocean Atmosphere Data Set (COADS; Slutz *et al.* [1985] , Woodruff *et al.* [1998]). Since 1982, SST is measured directly by satellite with global coverage, in contrast to Marine Air Temperature. The global data was separated in a "low-frequency" (inter-decadal) part and "high-frequency" (decadal) part, and missing data were filled in using different methods. Of relevance here is the procedure for the "high-frequency" interpolation. The global data was expanded in Empirical Orthogonal Teleconnections (EOT), which is similar to Empirical Orthogonal Functions (EOFs) with the exception noted below. The available ship and buoy data were projected onto these to help calibrate the satellite data. Prior to the availability of satellite data, there were large ocean areas without ship or buoy measurements. The available data were projected onto the leading EOTs deduced from satellite measurements after 1982. The influence by any measurement point is truncated beyond 8,000 km and damped beyond 5000km. These ranges of influence are larger than can be justified, but were necessitated by the sparse coverage. GISS dataset, for example, allows a single measurement to influence other grid points only up to 1200 km based on a correlation analysis of the data points (Hansen *et al.* [1999]). By this means, ocean SST data between 60 S and 60 N appear to be more geographically complete than land surface temperature data, and they greatly influence the global mean temperature used in IPCC AR4 report (Solomon *et al.* [2007]). Recently, Thompson *et al.* [2008] found that the global temperature data used in IPCC AR4 report is problematic during the Second World War, when British ships were replaced by US ships. The US ships measured SST using engine-water intake, which tended to be warmer than the British method of measuring SST on deck from water drawn up using buckets. The authors argued that this might account for the anomalous warming seen in the global temperature displayed in the AR4 report in the 1940s and the subsequent cooling as British ships resumed measurement in mid 1940s. This warming and cooling were suggested from time to time by some, perhaps erroneously, to be of solar origin, arguing that they were not expected from greenhouse trends. In our current study, the years 1942-1950 are deleted from our record as problematic years not yet adjusted in the data record, according to Thompson *et al.* [2008] . Their removal resolved much of the sensitivity we were encountering with the historical data with respect to the length of record analyzed.

Additionally, because of sparse data, the ERSST data were heavily damped before 1880, but it is claimed that after 1880, the signal strength was more consistent over time. We originally performed our calculation only for the period 1880-2007. Later when we repeated the calculation for the whole period 1854-2007, the results have very little difference in the overlapped period. Hence the full record, encompassing 14 solar cycles, are shown in Figure 1, although we do not have confidence in the spatial patterns of the response before 1880.

3. Composite-Mean Difference Projection method

We use the method of Composite-Mean Difference (CMD) Projection of Camp and Tung [2007a] . A similar but more sophisticated method is available in the form of Linear Discriminant Analysis (LDA) (Schneider and Held [2001]; Tung and Camp [2008] ; see also Camp and Tung [2007b]), but we chose the present simpler method for the greater ease with which others can reproduce our results, and because it is more intuitive. Briefly, this method separates temperature data into two groups, the solar max group and the solar min group. The separation is done objectively according to the TSI, to be discussed below. A global spatial pattern is obtained by composite-mean difference. The original data is then projected onto this CMD spatial pattern, resulting in a time series, which may or may not vary in phase with the solar (TSI) time series. The method is successful when the correlation is high. The correlation of these two time series is tested using a Monte-Carlo simulation. The unknown atmospheric population distribution is estimated by bootstrap re-sampling with replacement of the original temperature data, by assigning a year to either a solar max or solar min group randomly while preserving the number of years in each group. The exact CMD Projection method is applied to this synthetic data to produce a time series. The percentage of the time when this randomly generated time series has a correlation coefficient with the TSI equal to or higher than the observed one in magnitude is noted, and this number is often less than 0.02%. To take into account the inherent autocorrelation of the climate data, the re-sampling is repeated using a block of L years, where the length of L is to be determined by the autocorrelation time of the time series. Since L is not known a priori, we simply repeat the calculation for L=1,2,3,….,10, 11, 12 etc, and report the lowest confidence level obtained, which occurs at L=10. There is however not much change (less than 0.02%) between L=1 and L=10 for the decadal signal under study. The same holds true when we repeat our previously published results in Camp and Tung [2007a] and Tung *et al.* [2008], using L=10 instead of L=1. That is, all results previously deemed to be statistically significant at above 95% confidence level remain so using the moving-block re-sampling method.

Figure 1 shows the global mean (from 60 S to 60 N), annual mean SST from ERSST described above for the period 1854-2007, along with the annual mean TSI from Lean *et al.* [2005] and Wang *et al.* [2005] extended to 2007 and kindly provided to us by J. Lean. It is visually apparent that there exist *non-uniform* trends in both the SST and the TSI. There was a severe cooling of over 0.6K in the globally averaged SST in a short period of time from 1895 to 1910. Then the SST warmed by an even larger amount of 0.8K from 1910 to 1945. In 1945 there was the sudden anomalous drop in SST studied by Thompson *et al.* [2008] , before the modern global warming of 0.5K until 2007. This latest warming is usually attributed to the increase in greenhouse gases. The warming from 1910-1945 is sometimes attributed to the solar forcing, as the TSI coincidentally also increased during this period (see Figure 1). The solar max of 1910 was abnormally weak and the solar max of 1955-1960 was abnormally strong, and there was a general increasing trend in between. We will show however that this trend in TSI during the period 1910-1945 was too weak to account for the "observed" warming, which was likely due to bad data.

4. To detrend or not detrend:

In the period 1959-2004 previously analyzed by Camp and Tung [2007a] , the TSI from Lean *et al.* [2005] has no trend. In the longer term record we are analyzing here, the presence of the non-uniform trend, also from Lean *et al.* [2005] , makes some solar max TSI values in an earlier period lower than even the solar min TSI values in the more recent period. Since from physical grounds, it is the absolute irradiance that matters, with the higher TSI warming the earth more than the lower TSI does, it is not clear that a trend *should* be removed to center the TSI data. To compound the problem, the magnitude of the trend in TSI is uncertain and is currently under debate; see the IPCC AR4 report (p132, Forster *et al.* [2007]). We have decided not to detrend but to instead implement a *pair-wise differencing* procedure. We divide the TSI time series into sub-periods each containing just one whole solar cycle (with one solar max and one solar min). Since there is very little TSI trend within a decadal period, the solar max (min) years are defined as the years when the TSI is 0.06 Wm^{-2} above (below) the mean TSI for that particular short subperiod. (The 0.06 Wm^{-2} threshold was introduced by Camp and Tung [2007a] , so as not to count the years as either solar max or solar min when their TSI variations are within ~10% from the mean peak variation of ±0.6 Wm^{-2}.) This grouping/identification is objectively done for each solar-cycle period. The CMD is performed on the SST data one solar-cycle period at a time, by taking the difference between the temperature at solar max years and at solar min years. This difference for each solar cycle period is then averaged over all solar cycles in the longer data record. This method works well even with un-detrended data when the secular trends are small. During the last three decades, however, somewhat different results are found when a sub-period is defined as solar max following a solar min vs solar min following a solar max. This problem is remedied by the procedure of *pair-wise differencing with shift*, as described below.

The monotonic positive trend in the surface temperature in the recent decades may be due to forcing agents other than the TSI. An obvious candidate is the increase in greenhouse gases. To remove this contamination, we perform the above-described pair-wise differencing with the following modification. A whole solar-cycle sub-period is first defined as solar min following solar max. Then we repeat the procedure but by defining a whole solar-cycle sub-period as solar max following solar min. This is done by shifting the years comprising a solar cycle forward by half a cycle. The CMD spatial pattern that we will use is obtained by averaging the patterns obtained with these two definitions over this one and a half period. If there is a positive 5-10 year trend that exists within a solar cycle, it would manifest itself by giving a higher CMD warming if the solar max follows the solar min than if the solar min follows the solar max. The averaging then eliminates the short-term trend that might be present within a solar cycle, as the positive and negative contribution of the trend to the CMD cancels itself locally (within that one and a half solar cycles). Inter-decadal variations are not removed. Previously, in Camp and Tung [2007a] , the linear trend that exists in the temperature record of 1959-2004 was removed by linear detrending. This is not feasible in the 150-year data, as no single linear trend exists. Piecewise linear trend removal introduces artificial jumps in temperature, which is undesirable. Our method of pair-wise differencing with shift works very well and greatly reduces the sensitivity we have had in our previous trials with trend removal.

5. CMD Projection.

Figure 2 shows the longitude-latitude distribution of warming and cooling obtained by CMD (*pair-wise differencing with shift*), as described in the previous section, for the period 1854-2007. The spatial distribution prior to 1880 is probably not as reliable. Therefore we repeated the calculation using the period 1880-2007, shown in Figure 3. The difference between the two relate mostly to the fact that the amplitude of the warming and cooling centers are slightly larger in Figure 3, due probably to the fact that the data prior to 1880 were heavily damped in the dataset. This spatial CMD pattern is denoted by $P_1(\mathbf{x})$. In the CMD Projection method, the original SST data is expanded in an empirical-orthogonal-function expansion as:

$$T(x,t) = \sum C_n(t) P_n(x). \tag{1}$$

The orthogonality of the spatial modes is enforced by the definition of the projection coefficients:

$$Cj(t) = \frac{\int T(x,t) Pj(x) dx}{\int P_j^2 dx}. \tag{2}$$

So when $C_1(t)$ is defined this way, the "solar-cycle" mode $P_1(x)$ is orthogonal to sum of all the remaining modes, which theoretically included all other variability and noise. The lower panel in Figure 2 shows the projected time series $C_1(t)$ in blue. It is the time variation of the solar response in the SST data corresponding to the spatial pattern shown in the top panel. For convenience of presentation, $C_1(t)$ is additionally normalized by the global mean of $P_1(\mathbf{x})$, so that the magnitude of $C_1(t)$ is interpretable as the magnitude of the globally averaged SST variation in response to the solar TSI variation.

Looking at the time series of solar-cycle response in Figures 3, we see that solar max *warms* relative to solar min in globally averaged SST in the 13 solar cycles examined. There was not a phase reversal in 1920 or during any other period. The amplitude of the global SST response is about 0.1 C per 1 Wm^{-2} (the scale of TSI and $C_1(t)$ are scaled 1 Wm^{-2} to 0.1 C, to facilitate this comparison). There are however a couple cycles where the amplitude is smaller, and this can usually be attributed to questionable data. When regressed over all cycles (excluding however the period 1942-1950 mentioned earlier), including periods of remaining bad data, the warming in globally averaged SST (over 60 S and 60 N) is κ~0.085 C per 1 Wm^{-2} for the period 1880-2007. This amplitude is about the same that found by White *et al.* [1997] for the period 1900-1991. The solar cycle response amplitude found here for the SST is about 60-70% of that found in the land-ocean average found by Tung *et al.* [2008] for the *in-situ* data of GISS and HadCRUT3. This finding is consistent with the value of κ=0.12 C per Wm^{-2} found for the land-ocean average in those two in-situ datasets because warming is usually stronger over continents. The ratio of the present ocean average vs global average of land and oceans is even smaller in the recent reanalysis data, also shown in Tung *et al.* [2008] , which included areas poleward of 60 N and S, with amplified warming, not included in the *in-situ* data.

There is a severe cooling trend after the eruption of Santa Maria in October of 1902 that lasted more than a decade, longer than can be expected from volcano aerosol cooling. Interestingly, this cooling does not project onto the solar response pattern, indicating that this severe cooling may be due to noise or more likely bad data, and is effectively filtered out by our projection method. The decade after WWII produced a solar max response that is smaller than expected from the TSI. The global SST is actually very warm during that solar max (see the black line in Figure 1), but it does not project onto the solar response spatial pattern. This is an indication that the spatial pattern of the SST during that decade is not consistent, as the mix of British and US ships was changing (Thompson *et al.* [2008]). The WWII years likewise does not project significantly onto the solar response spatial pattern (not shown) if the latter is obtained for the period 1854-2008 with the WWII years excluded, showing that the warming and cooling during that period were not solar related. Nevertheless the erroneous temperature discontinuity is so large that if the WWII years had been included in our calculation of the spatial patterns it would have contaminated that pattern.

6. Statistical tests

The correlation coefficient ρ between the temperature response $C_1(t)$ and the TSI is about 0.69 for the period 1880-2007 and 0.65 for the period 1854-2008, both quite high for such a long data record and extremely unlikely to be producible by chance if there were no solar-cycle signal in the SST (the null hypothesis). Figure 4 shows the distribution of ρ in 10,000 synthetic SST time series generated using the method of bootstrap with replacement, to be described now. The relationship between the TSI and years is not randomized but held fixed as the real values, so the grouping of years into the solar groups remains the same as described in section 3. However, the temperature value for a particular year, say, 1880, is drawn randomly from a year (which could happen to be 1920) in the real SST data record. Afterwards that year is returned to the SST record and another year is drawn randomly from this entire SST data to be assigned to 1881 and so on. (The year chosen in a previous step needs to be returned to the pool before another year is chosen; otherwise later draws would not be independent of the early ones. For example, if the years were not returned to the pool and N-1 years were chosen, then the N^{th} year would be dependent on the previous N-1 years.) In this way, the years are populated by SST values. The original association of the temperature with the solar groups is destroyed, but the number of years in each solar group is maintained. The CMD Projection method described in section 3 is then applied to this synthetic SST data to generate a time series $C_1(t)$, which is then correlated with the TSI time series to yield a correlation coefficient. Repeating this procedure many times (e.g. 10,000), one can then establish a confidence level to reject the null hypothesis by seeing how many synthetic correlation coefficients are less than the observed value.

To take into account the fact that our temperature data may be serially correlated (Zwiers [1987]; Zwiers [1990]) , the above bootstrap method is modified using the so-called moving-block bootstrap (Efron and Tibshirani [1993]; Lahiri [2003]; Leger *et al.* [1992]; Wilks [1997]). Blocks of L successive data values are re-sampled instead of re-sampling individual data values. The value of L is defined so that data values of L-distance or longer away from each other are essentially independent. Generally it is difficulty to theoretically determine an appropriate block length L (Leger *et al.* [1992]). However, under the assumption that the original time series is modeled as a first-order autoregressive process, Wilks [2006] , Chapter 5, has suggested that a good choice of the block length L is given by:

$$L = (n - L + 1)^{2/3(1-n'/n)},$$

where n is the sample size, $n' = n(1-\rho_1)/(1-\rho_1)$ is the approximated effective sample size and ρ_1 is the lag-1 autocorrelation coefficient. For our problem, the block length L calculated using the above formula varies from 1 to about 20 years depending on the spatial location. Since the temperature data may not follow AR(1) processes very well, the above estimate for L may still not be accurate. The method that is adopted here is actually quite simple: we repeat the calculation for each value of L and conservatively take the value of L that yields the lowest level of statistical confidence. This occurs at 10 years. We still find that very few of the 10,000 synthetic SST time series achieve a correlation equal to or higher than the observed value. Thus we have effectively ruled out the null hypothesis that our method can by random chance generate an apparent "signal" highly correlated with the TSI when no real solar signal exists in the data.

One may be suspicious of this high confidence level and question whether it can be caused by the fact that it is helped by the existence of the long-term trend in the observed time series, with the temperature in earlier decades before WWII lower than in the more recent decades after the war, while in the synthetic data there is no consistent trend because of the scrambling of the years. It turns out that unlike the regression coefficient κ, the correlation coefficient is not sensitive to the presence of trend in $C_1(t)$. When we remove the trend in $C_1(t)$ before correlating it with TSI, ρ is changed only slightly. The results of such a calculation are indicated in Figure 4.

7. Spatial Features in Ocean Basins.

We will next discuss the features in Figure 3, obtained using the better data since 1880. It shows that the response over oceans has both warming and cooling distributed in some characteristic patterns, more so than the warming over continents found in our previous work. The ocean area-averaged temperature is therefore smaller than the local

SST anomaly, which ranges from -0.2 to +0.2 C. In the Atlantic Ocean, the tropics is cold south of the Equator but warm a little north of it. Northwestern Atlantic is cold. Indian Ocean is warm. These features are robust. Being a small ocean basin, the robust basin-wide warming in Indian Ocean may indicate a radiative response to solar forcing, in contrast to the situation in the larger ocean basin of the Pacific, which is capable of fast dynamical responses involving coupled atmosphere and oceans (Meehl and Arblaster [2009]; Tourre *et al.* [2001]; White and Tourre [2003]).

In the Pacific Ocean, there is a robust warming center located in the Northwestern Pacific, and cooling off the west coast of the United States. There is generally cooling in tropical Eastern Pacific, with the exception of a thin warming strip located at the Equatorial Pacific, where the ENSO variance is large. The warming center in the Northwestern Pacific is robust, but the warming strip in the eastern Pacific is not (Compare Figures 2 and 3, and see later figures).

Previously, Van Loon *et al.* [2007] and Van Loon and Meehl [2008] studied specifically the spatial pattern in the Pacific during northern winter using the same ERSST data since 1854. They calculated their composite mean difference by taking the difference of the mean of the "solar peak years" (one year per solar cycle) and the climatology, in effect using only 14 degrees of freedom. The climatology was calculated over a different period than that from which the solar peak years were chosen (The period used in the climatology calculation was based on only thirty years, 1950-1979, in Van Loon *et al.* [2007] . A different twenty nine years, 1968-1996, was used in Van Loon and Meehl [2008]). Over the equatorial east Pacific, they found a cold-event (La Nina)-like condition, which was deemed statistically significant by the student-*t* test. Our Monte-Carlo test of bootstrap re-sampling cannot be applied to their methodology because there is only one data point in each solar cycle. There is no time series information on the response for us to test the similarity between the response and the forcing when only one year is used for each solar cycle. So we cannot refute the null hypothesis that the spatial pattern is not related to the solar cycle. The student-*t* test they used does not actually test if the signal is solar related; it merely tests if the mean of the solar peak years is significantly different from the mean of the years used in defining the "climatology". It is in this regard that the subjective choice of the years used in the calculation of climatology affects the student-*t* test result. Because the period, 1968-1996, chosen by Van Loon and Meehl [2008] for the climatology, is warmer, it yields a larger amplitude equatorial Pacific SST cold tongue when it is subtracted from the solar peak mean, and therefore it passes the student-*t* test. This is their best result, and is reproduced here in the top panel of Figure 5. The yellow contour encloses regions of statistical significance at 95% confidence level, and we see that the cold tongue at the eastern Pacific and a warm pool over the northwestern Pacific are both statistically significant, as discussed in detail by Van Loon and Meehl [2008] . This result, however, is not robust to either the choice of the so-called solar peak years and of the base period for the calculation of climatology. The middle panel in Figure 5 is done in the same way as in Van Loon and Meehl [2008] except that the peak solar years are chosen objectively according to the peaks in TSI. The spatial pattern is rather different—the La Nina pattern is disrupted---but nevertheless the eastern Pacific is cold and still statistically significant. This changes again when the proper climatology is taken, using the same period (1854-2007) as that from which the solar peak years were chosen. This is the most objective way for the composite difference and the result is shown in the bottom panel of Figure 5. None of the features in the Pacific is statistically significant by the student-*t* test.

The hypothesis that it is the solar peak years that causes the La-Nina like response in the equatorial Pacific (Van Loon and Meehl [2008]; Van Loon *et al.* [2007]) and that one or two years later the response switches to a El-Nino like pattern (Meehl and Arblaster [2009]) may still be correct, and appears to be supported by modeling results as reported in Meehl *et al.* [2009] . The observational support for this hypothesis is however not yet available. It is likely that 150 years of data are not long enough for us to separate out different behaviors in the first vs second years of a solar max.

The question of whether the equatorial Pacific responds to a warmer climate in a La Nina-like pattern or an El Nino-like pattern is under debate in the context of global warming. Vecchi *et al.* [2008] showed that the ERSST data we are using gives a long-term trend in the form of an El Nino-like pattern while a different SST dataset, HadISST, gives a La Nina-like pattern. They attributed the difference to the difference between the two datasets in two periods: the 1930s and the 1980s, which corresponded to periods of greatest change in "buckets-to-intake" correction of SST measurements previously implemented (i.e. prior to Thompson et al [2008]) and the beginning of SST retrievals using satellites.

8. Multi-decadal trend

Since our method does not involve detrending of temperature or TSI, there is a secular SST response seen in Figure 2 to the secular trend in the solar forcing. Generally the level of SST solar response is consistent with the level of TSI forcing, with periods of high SST associated with periods of high TSI. By regressing $C_1(t)$, using just the solar-min years, or just the solar-max years, or the entire time series, onto the years to determine the slope of the time series, the amplitude of the global SST trend arising from the solar influence is found to be about $0.004 \pm 0.0012^\circ C$ per decade for the period of 1854-2007 or $0.009 \pm 0.0017^\circ C$ per decade for the period 1880-2007. These bracket the solar trend over the last century, $0.007 \pm 0.001^\circ C$ per decade, reported by Lean and Rind [1998]. However, this slope of $C_1(t)$ is not a robust quantity since the actual trend is nonlinear. In order to set an upper bound on the solar forcing contribution to the warming trend, we give two maximum values, one using only peak solar max years, and one for peak solar min years: it warmed by 0.18 C from the solar max of 1909 to the solar max of 2002. During this period the global mean SST warmed by 0.89 C, and so no more than 20% of that may be attributed to solar forcing during this period. A larger warming of 0.21 C is found from the solar min of 1913 to the solar min of 2005. This last number, 0.21 C, is deemed the upper bound in the secular change in SST that can be attributed to solar forcing, first because that is the difference between the lowest and the highest temperatures in the solar min in the entire record and secondly because some greenhouse warming residue may arguably remain in $C_1(t)$ during the most recent solar cycle (possibly since the solar min in 2007 is the last half cycle analyzed) despite our best efforts in removing it. During this same period of time, the global mean SST warmed by 0.81 C, and so no more than 26% of it can be attributed to solar forcing. These are upper bounds; the true solar trend is probably lower. These changes in SST associated with the inter-decadal changes in solar forcing are quite modest, and in no way can account for the observed warming trend of in SST during the last century (see Figure 1). The latter must have been caused by other forcing agents, including anthropogenic ones.

9. Volcano, ENSO and greenhouse warming contamination; a Multi-CMD Analysis.

When there is long enough data, within-group variances caused by volcanoes and El Nino-Southern Oscillation (ENSO), which are not consistently correlated with the solar cycle, are hopefully greatly reduced by the composite means and by the differencing of the two groups. Nevertheless how well these variances are removed has always been a concern. In the analysis shown in Figures 2 and 3, no volcano years were removed before processing, unlike the procedure in Camp and Tung [2007a] . The result is not so different from that obtained (not shown) by excluding the volcanic years from the analysis. The time series $C_1(t)$ is highly correlated with the solar index ($\rho = 0.69$), and not correlated with the volcanic aerosol index (Sato *et al.* [1993]); the latter correlation coefficient, $\rho_{AI} = -0.08$, is practically zero. We will show directly below that volcano contamination is indeed very small. Global warming due to increases in greenhouse gases is another important contamination to the solar signal. Nonetheless the method that we introduced in section 4 to obtain the solar signal reduces this contamination greatly, as we will quantify below. ENSO is a prominent variability in the Pacific Ocean, and can affect significantly the SST patterns studied here, more so than the land-ocean patterns studied previously. For the present study, extreme ENSO years, defined as when the winter (DJF) mean Cold Tongue Index (CTI) exceeds 1.2 C in magnitude, are excluded in the analysis presented in sections 3 and 4. The resulting $C_1(t)$ has a correlation coefficient with the annual mean CTI index of -0.13 for the period 1880-2007, which is small enough for the ENSO contribution to the derived solar signal to be negligible. To verify that these contaminations are already small in what we have produced, we shall now try to separate out these four deterministic signals and show that our results on the solar-cycle response are not changed.

In a typical error analysis, one assumes that the data consist of the signal under study and a remainder, called "noise". A noise model needs to be constructed; usually either a random white-noise model or a red-noise model is assumed. As pointed out by North and Stevens [1998] , neither of these noise models is appropriate because the climate data contain prominent deterministic signals such as ENSO and volcano aerosols, and they need to be taken into account explicitly. We shall assume that our data $D(\mathbf{x},t)$ consist of multiple deterministic signals plus a random noise, in the following form:

$$D(x,t)=\theta_S(t)p_S(x)+\theta_E(t)p_E(x)+\theta_V(t)p_V(x)+\theta_A(t)p_A(x)+R(x,t), \tag{3}$$

where the p 's are the *true* (unknown to us) spatial patterns of the climate influences and the θ 's represent their time behavior. The subscripts S,E,V and A indicate the solar, ENSO, volcanic and anthropogenic greenhouse gas increases, respectively. $R(x,t)$ is the residual noise, assumed to be random. Superficially this assumed form for the data appears to be quite similar to what is assumed in multiple regression methods. However, the least-square multiple regression method minimizes the sum of squares of $R(x,t)$, while our estimate of the true spatial patterns are obtained by assuming that the means of $R(x,t)$ itself to be small. Our assumption appears justified in a long data record, where if enough deterministic signals are taken out from $D(\mathbf{x},t)$, the remainder can be assumed to be approximately random with very small mean.

Here we first perform the CMD procedure four times on the data, each with the two groups selected according to different forcing agent (thus the years contributing to calculate the CMD may vary for each climate signal), to establish the following linear equations:

$$\begin{bmatrix} P_1^S \\ P_1^E \\ P_1^V \\ P_1^A \end{bmatrix} = \begin{bmatrix} 1 & \frac{\alpha_E^S}{\alpha_E} & \frac{\alpha_V^S}{\alpha_V} & \frac{\alpha_A^S}{\alpha_A} \\ \frac{\alpha_S^E}{\alpha_S} & 1 & \frac{\alpha_V^E}{\alpha_V} & \frac{\alpha_A^E}{\alpha_A} \\ \frac{\alpha_S^V}{\alpha_S} & \frac{\alpha_E^V}{\alpha_E} & 1 & \frac{\alpha_A^V}{\alpha_A} \\ \frac{\alpha_S^A}{\alpha_S} & \frac{\alpha_E^A}{\alpha_E} & \frac{\alpha_V^A}{\alpha_V} & 1 \end{bmatrix} \begin{bmatrix} \alpha_S p_S \\ \alpha_E p_E \\ \alpha_V p_V \\ \alpha_A p_A \end{bmatrix} + \begin{bmatrix} \alpha_R^S \\ \alpha_R^E \\ \alpha_R^V \\ \alpha_R^A \end{bmatrix}, \tag{4}$$

where the $P_1^{'}s$ are the (known) composite-mean differences of the data $D(x,t)$ and α_R 's are the (unknown) CMD of the noise $R(x,t)$. The $\alpha_S, \alpha_E, \alpha_V, \alpha_A$ and are the CMD of the four θ 's , which we will assume to be the same as those calculated using the prescribed forcing index for each phenomenon. The superscripts S,E,V and A indicate by which forcing agent the two groups are defined when calculating the CMD. They are omitted when they are the same as the subscript. We let $\hat{p}$ be the *estimate* of the true spatial pattern $p(x)$ obtained by ignoring the noise CMD α_R:

$$\begin{bmatrix} 1 & \frac{\alpha_E^S}{\alpha_E} & \frac{\alpha_V^S}{\alpha_V} & \frac{\alpha_A^S}{\alpha_A} \\ \frac{\alpha_S^E}{\alpha_S} & 1 & \frac{\alpha_V^E}{\alpha_V} & \frac{\alpha_A^E}{\alpha_A} \\ \frac{\alpha_S^V}{\alpha_S} & \frac{\alpha_E^V}{\alpha_E} & 1 & \frac{\alpha_A^V}{\alpha_A} \\ \frac{\alpha_S^A}{\alpha_S} & \frac{\alpha_E^A}{\alpha_E} & \frac{\alpha_V^A}{\alpha_V} & 1 \end{bmatrix} \begin{bmatrix} \alpha_S \hat{p}_S \\ \alpha_E \hat{p}_E \\ \alpha_V \hat{p}_V \\ \alpha_A \hat{p}_A \end{bmatrix} = \begin{bmatrix} P_1^S \\ P_1^E \\ P_1^V \\ P_1^A \end{bmatrix}. \tag{5}$$

The error of the estimations can be found by computing

$$\begin{bmatrix} \alpha_S \hat{p}_S \\ \alpha_E \hat{p}_E \\ \alpha_V \hat{p}_V \\ \alpha_A \hat{p}_A \end{bmatrix} - \begin{bmatrix} \alpha_S p_S \\ \alpha_E p_E \\ \alpha_V p_V \\ \alpha_A p_A \end{bmatrix} = M^{-1} \begin{bmatrix} \alpha_R^S \\ \alpha_R^E \\ \alpha_R^V \\ \alpha_R^A \end{bmatrix}, \tag{6}$$

where M^{-1} is the inverse of the matrix in Eq. (5). It can be seen that the error in the estimated spatial patterns is now caused solely by the random noise, in particular, the CMD of the noise, which is small.

Since the variations of different climate forcings are usually not in phase, the non-diagonal elements of the matrix M (and thus M^{-1}) are all expected to be small, as they turn out to be in our case. Eq. (6) then implies that there is very little cross-contamination of errors. The CMD of the random noise in the right-hand side of Eq.(6) should be small if the data record is long. However even in a long record there may not be enough occurrences of volcano eruptions to make the volcano-CMD of the noise to be small. Any such error due to poor volcano sampling will stay as an error in the estimated volcano spatial pattern, and not cross-contaminate the solar spatial pattern estimate.

Shown from the top to bottom panels in Figure 6 are the estimated spatial patterns $\alpha_S \hat{p}_S$, $\alpha_E \hat{p}_E$, $\alpha_V \hat{p}_V$ and $\alpha_A \hat{p}_A$ obtained for the period 1880-2007. Based on each climate forcing, we pick up the years and group them to compute the CMD as follows (the years 1942-1950 are always removed beforehand): The solar max (min) years are defined according to the TSI index as having a TSI greater (smaller) than 0.06 Wm^{-2} of the local mean of a complete solar cycle. The warm (cold) ENSO years are defined as the years when the annual mean CTI is greater than 0.25 C (less than -0.25 C). The volcano years are: 1883-1885, 1902-1904, 1963-1965, 1982-1984 and 1991-1993, including three years after each major eruption indicated in Figure 1. The non-volcanic group contains years when the annual mean aerosol index is no larger than 0.005 optical depths. The two anthropogenic groups comprise the years when the global mean CO_2 mixing ratios (Hansen *et al.* [1998]) are 10 ppm above or below the mean of the entire period of data record, 1880-2007.

It is worthwhile to point out that Eq. (4) is derived by applying the simplest composite mean differencing. For example, P_1^S is the simple difference between the mean temperature of all the solar max years and that of all the solar min years during the whole period. This P_1^S (not shown) is not a good estimate to the true solar cycle spatial pattern, as it contains other deterministic signals such as volcano aerosols and greenhouse gas warming. (Recall that the error in the solar spatial pattern obtained by the simple CMD method is
$P_1^S - \alpha_S p_S = \alpha_E^S p_E + \alpha_V^S p_V + \alpha_A^S p_A + \alpha_R^S$.)
It is only used as an intermediate step in the calculation. P_1^S is very different from the estimate, $\widehat{p_S}(x)$, which removes these deterministic contaminations as shown above. The surprising finding is that this estimate obtained via Multiple-CMD Inversion (in the top panel of Figure 6) is very close to that obtained in section 4 using the single *pair-wise differencing with shift* method (shown in Figure 3). The latter method is effective in removing the secular trend, presumably due to the anthropogenic greenhouse gases also removed in the Multiple-CMD Inversion. The length of the record serves to averaging out the volcanic and ENSO contaminations, yielding very small differences in the two spatial patterns.

10. Conclusions

It is often thought that the response to solar cycle is too weak at the surface to be detectable, and that even if a signal is claimed to have been found its statistical significance cannot be established. Using 150 years of sea-surface temperature data from 1854 to 2007 and an objective method, we found a robust signal of warming over solar max and cooling over solar min, with high statistical significance in the time domain. The amplitude of the signal in the SST averaged over the ocean areas between 60 N and 60 S is ~0.085 C per Wm^{-2} of the change in TSI, which is about 70% that found in land-ocean averages (~0.12 C per Wm^{-2}) found in the recent in-situ data by Tung *et al.* [2008] , as to be expected because response over continents and over the Arctic is known to be larger.

Volcanic eruptions tend to have a significant contribution to the decadal period peak in any spectral analysis, and therefore contamination of the solar-cycle signal by volcanic signal has been a long standing concern. Using 150 years of data we have now shown that the volcanic contamination is negligible using our method of *pair-wise differencing with shift*. This is further confirmed using a new method of Multiple-CMD Inversion, similar to the multiple regression method, where the deterministic volcanic signals are separated out.

Our method of projecting the observed data onto a consistent spatial pattern determined by composite-mean difference of the whole period appears to be effective in reducing contamination by short periods of bad data, which tend to have inconsistent spatial patterns. This effect is in contrast to that of the method of (multiple) regression using least-square fit of the time series, which is affected by outliers (which may likely be caused by bad data).

In the method of multiple regressions as applied to solar variation by previous authors, an index of solar forcing as a function of time, often in the form of TSI or sunspot number, needs to be prescribed, and the resulting response is assumed to vary in time in exactly the same way as the imposed index, albeit with the possibility of a lag. Our method of CMD Projection depends only on the classification of years into the solar max or solar min group, and does not require that we know the detailed variation of the total solar irradiation, nor its long-term trend. In this way we bypass the controversy concerning the magnitude of the solar forcing trend in these 150 years. Assuming that multi-decadal SST response has the same spatial pattern as the decadal response, we additionally obtain a secular century trend; the latter is consistent with Lean's reconstruction of solar forcing. Our result shows that less than a quarter of the observed temperature trend can be attributed to solar forcing.

Acknowledgment

We thank Dr. Charles D. Camp for helpful suggestions on the moving block bootstrap test. We are also grateful to Dr. Jerald Meehl and two other reviewers for very helpful comments. The research is supported by National Science Foundation, Climate Dynamics Program, under grant ATM 0808375.

References

Allen, R. J., 2000: ENSO and Climate Variability in the Past 150 Years. *El Nino and the Southern Oscillation, Multiscale Variability and Global and Regional Impacts*, H. F. Diaz and V. Markgraf, Eds., Cambridge University Press, 1-55.

Camp, C. D. and K. K. Tung, 2007a: Surface warming by the solar cycle as revealed by the composite mean difference projection. *Geophysical Research Letters*, **34,** L14703, doi:10.1029/2007GL030207.

——, 2007b: The influence of the solar cycle and QBO on the late winter stratospheric polar vortex. *J. Atmos. Sci.*, **64,** 1267-1283.

Clayton, H. H., 1940: The 11-year and 27-day solar periods in meteorology. *Smithsonian Miscellaneous Collections*, **39,** 20pp.

Efron, B. and R. J. Tibshirani, 1993: *An Introduction to the Bootstrap*. Cahpman and Hall, 436 pp.

Forster, P. M., V. Ramaswamy, P. Artaxo, T. Berntsen, R. Betts, D. W. Fahey, J. M. Haywood, J. Lean, D. C. Lowe, G. Myhre, J. Ngang, R. Prinn, M. Rnga, M. Schutz, and R. Van Dorland, 2007: Changes in atmospheric constituents and in radiative forcing. . *Climate Change 2007: The Physical Science Basis. Contribution of Working Group I to the Fourth Assessment Report of the Intergovernmental Panel on Climate Change*, S. Solomon, D. Qin, M. Manning, Z. Chen, K. B. Marquis, K. B. Averyt, M. Tignor, and H. L. Miller, Eds., Cambridge University Press.

Hansen, J., M. Sato, A. Lacis, R. Ruedy, I. Tegen, and E. Mathews, 1998: Climate forcings in the industrial era. *Proc. Natl. Acad. Sci. USA* **95**, 12753-12758.

Hansen, J., R. Ruedy, J. Glascoe, and M. Sato, 1999: GISS analysis of surface temperature change. *J. Geophys. Res.*, **104,** 30,997-31,022.

Hoyt, D. V. and K. H. Schatten, 1997: *The role of the sun in climate change*. Oxford University Press, 279 pp.

Lahiri, S. N., 2003: *Resampling Methods for Dependent Data*. Springer, 374 pp.

Lean, J., 2005: Living with a variable sun. *Phys. Today*, **58,** 32-38.

Lean, J. and D. Rind, 1998: Climate forcing by changing solar radiation. *Journal of Climate*, **11,** 3069-3094.

——, 2008: How natural and anthropogenic influences alter global and regional surface temperatures: 1889-2006. *Geophys. Research. Lett.*, **35**.

Lean, J., J. Beer, and R. Bradley, 1995: Reconstruction of Solar Irradiance since 1610 - Implications for Climate-Change. *Geophysical Research Letters*, **22,** 3195-3198.

Lean, J., G. J. Rottman, J. Harder, and G. Kopp, 2005: SORCE contributions to new understanding of global change and solar variability. *Sol. Phys.*, **230,** 27-53.

Leger, C., D. N. Politis, and J. P. Romano, 1992: Bootstrap technology and applications. *Technometrics*, **34,** 378-398.

Meehl, G. A. and J. M. Arblaster, 2009: A lagged warm event-like response to peaks in solar forcing in the Pacific region. *J. Climate.*, **in press**.

Meehl, G. A., J. M. Arblaster, K. Matthes, F. Sassi, and H. Van Loon, 2009: Amplifying the Pacific climate system response to a small 11-year solar cycle forcing. *Science*, **325,** 1114-1118.

North, G. R. and M. J. Stevens, 1998: Detecting climate signals in the surface temperature record. *J. Climate*, **11,** 563-577.

Sato, K., J. E. Hansen, M. P. McCormick, and J. B. Pollack, 1993: Stratospheric aerosol optical depths, 1850-1990. *J. Geophys. Res.*, **98,** 22987-22994.

Scafetta, N. and R. Willson, 2009: ACRIM-gap and TSI trend issue resolved using a surface magnetic flux TSI proxy model. *Geophysical Research Letters*, **36,** doi:10.1029/2008GL036307.

Schneider, T. and I. M. Held, 2001: Discriminants of twentieth-century changes in earth surface temperatures. *Journal of Climate*, **14,** 249-254.

Slutz, R. J., S. J. Lubker, J. D. Hiscox, S. D. Woodruff, R. L. Jenne, D. H. Joseph, P. M. Steurer, and J. D. Elms, 1985: Comprehensive Ocean-Atmosphere Data Set; Release 1. C. R. P. NOAA Environmental Research Laboratories, Boulder, CO, Ed., 268pp.

Smith, T. M. and R. W. Reynolds, 2003: Extended reconstruction of global sea surface temperatures based on COADS data (1854-1997). *J. Climate.*, **16,** 1495-1510.

——, 2004: Improved extended reconstruction of SST (1854-1997). *J. Climate.*, **17,** 2466-2477.

Smith, T. M., R. W. Reynolds, T. C. Peterson, and J. Lawrimore, 2008: Improvements to NOAA's Historical Merged Land-Ocean Surface Temperature analysis (1880-2006). *J. Climate.*, **21,** 2283-2296.

Solomon, S., D. Qin, M. Manning, Z. Chen, M. Marquis, K. B. Avery, M. Tignor, and H. L. Miller, 2007: Climate Change 2007: The Physical Science Basis.

Stevens, M. J. and G. R. North, 1996: Detection of the climate response to the solar cycle. *J. Atmos Sci.*, **53,** 2594-2608.

Thompson, D. W. J., J. J. Kennedy, J. M. Wallace, and P. D. Jones, 2008: A large discontinuity in the mid-twentieth century in observed global mean surface temperature. *Nature*, **453,** doi:10.1038/nature06982.

Tourre, Y. M., B. Rajagopalan, Y. Kushnir, M. Barlow, and W. B. White, 2001: Patterns of coherent decadal and interdecadal climate signals in the Pacific Basin during the 20th century. *Geophys. Research. Lett.*, **28,** 2069-2072.

Tung, K. K. and C. D. Camp, 2008: Solar-cycle warming of the earth's surface in NCEP and ERA-40 data, a Linear Discriminant Analysis. *J. Geophys. Res.*, **113,** D05114, doi:10.1029/2007JD009164.

Tung, K. K., J. Zhou, and C. D. Camp, 2008: Constraining model transient climate response using independent observations. *Geophys. Research. Lett.*, **35**.

Van Loon, H. and G. A. Meehl, 2008: The response in the Pacific to the sun's decadal peaks and contrasts to cold events in the Southern Oscillation. *J. Atmos & Solar-Terres. Phys*, **70,** 1046-1055.

Van Loon, H., G. A. Meehl, and D. J. Shea, 2007: Coupled air-sea response to solar forcing in the Pacific region during northern winter. *J. Geophys. Res.*, **112,** D02108, doi:10.1029/2006JD007378.

Vecchi, G. A., A. Clement, and B. J. Soden, 2008: Examining tropical Pacific's response to global warming. *Eos*, **89,** 81-83.

Wang, Y.-M., J. Lean, and N. R. Sheeley Jr, 2005: Modeling the Sun's magnetic field and irradiance since 1713. *Astrophys. J.*, **625,** 522-538.

White, W. B. and Y. M. Tourre, 2003: Global SST/SLP waves during the 20th century. *Geophys. Research. Lett.*, **30,** doi:10.1029/2003GL017055.

White, W. B., J. Lean, D. R. Cayan, and M. D. Dettinger, 1997: Response of global upper ocean temperature to changing solar irradiance. *J. Geophys. Res.-Oceans*, **102,** 3255-3266.

Wilks, D. S., 1997: Resampling hypothesis tests for autocorrelated fields. *J. Climate.*, **10,** 65-82.

——, 2006: *Statistical Methods in the Atmospheric Sciences*. Second ed. Academic Press, 627 pp.

Woodruff, S. D., H. F. Diaz, J. D. Elms, and S. J. Worley, 1998: COADS Release 2 data and metadata enhancements for improvements of marine surface flux fields. *Phys. Chem. Earth*, **23,** 517-526.

Zwiers, F. W., 1987: Statistical considerations for climate experiments, Part II: Multivariate tests. *J. Climate and Applied Meteorology*, **26,** 477-487.

——, 1990: The effect of serial correlation on statistical inferences made with resampling procedures. *J. Climate and Applied Meteorology*, **3,** 1452-1461.

Figure Legends

Figure 1. Sea-Surface Temperature, averaged from 60S-60N over the ocean areas, from NOAA's ERSST dataset from 1854-2008, top. Solar constant (Total Solar Irradiance) from Lean *et al.* [2005] and Wang *et al.* [2005] , bottom.

Figure 2. For the period 1854-2007, the spatial pattern of SST obtained from CMD in the top panel. The time series obtained by projecting the original data onto this pattern is shown in the lower panel in blue. The TSI index is shown in red. The correlation coefficient of the two curves is given by $\rho=0.65$, which is statistically significant at above 95% confidence level (99.99%) using bootstrap re-sampling with 10-year blocks of data.

Figure 3. Same as Figure 2 except for the period 1880-2007.

Figure 4. Distribution of the magnitude of correlation coefficients between the projected SST time series $C_1(t)$ and the solar TSI index, obtained using synthetic data generated by the bootstrap resampling Monte-Carlo method. (a) for the period 1854-2007, (b) for the period 1880-2007. The solid vertical line is the observed ρ, and the dashed vertical line is the observed ρ obtained when the data was first detrended, denoted by ρ'. Note that here $C_1(t)$ is not normalized by the global mean of $P_1(\mathbf{x})$, which explains why the distribution is not bimodal.

Figure 5. Difference in SST between the mean of the "solar peak years" (indicated at the top of the figure) during January to February over the period 1854-2007 and the "climatology" (computed for periods indicated along the left edge of the figure). Yellow contour enclose regions of 95% confidence level; dashed black contour encloses regions of 99% confidence level. Top panel: solar peak years determined by peaks in sunspot number; climatology determined by the period 1968-1996 chosen by Van Loon and Meehl [2008] . Middle panel: solar peak years determined by peaks in TSI; climatology determined by the period 1968-1996; bottom panel: solar peak years determined by the peaks in TSI; climatology determined by the whole period of data record, 1854-2007.

Figure 6: Spatial pattern in SST response derived using Muliple-CMD Inversion method for, from the top to bottom panels: solar cycle, ENSO, volcano aerosols, and greenhouse gas increases.

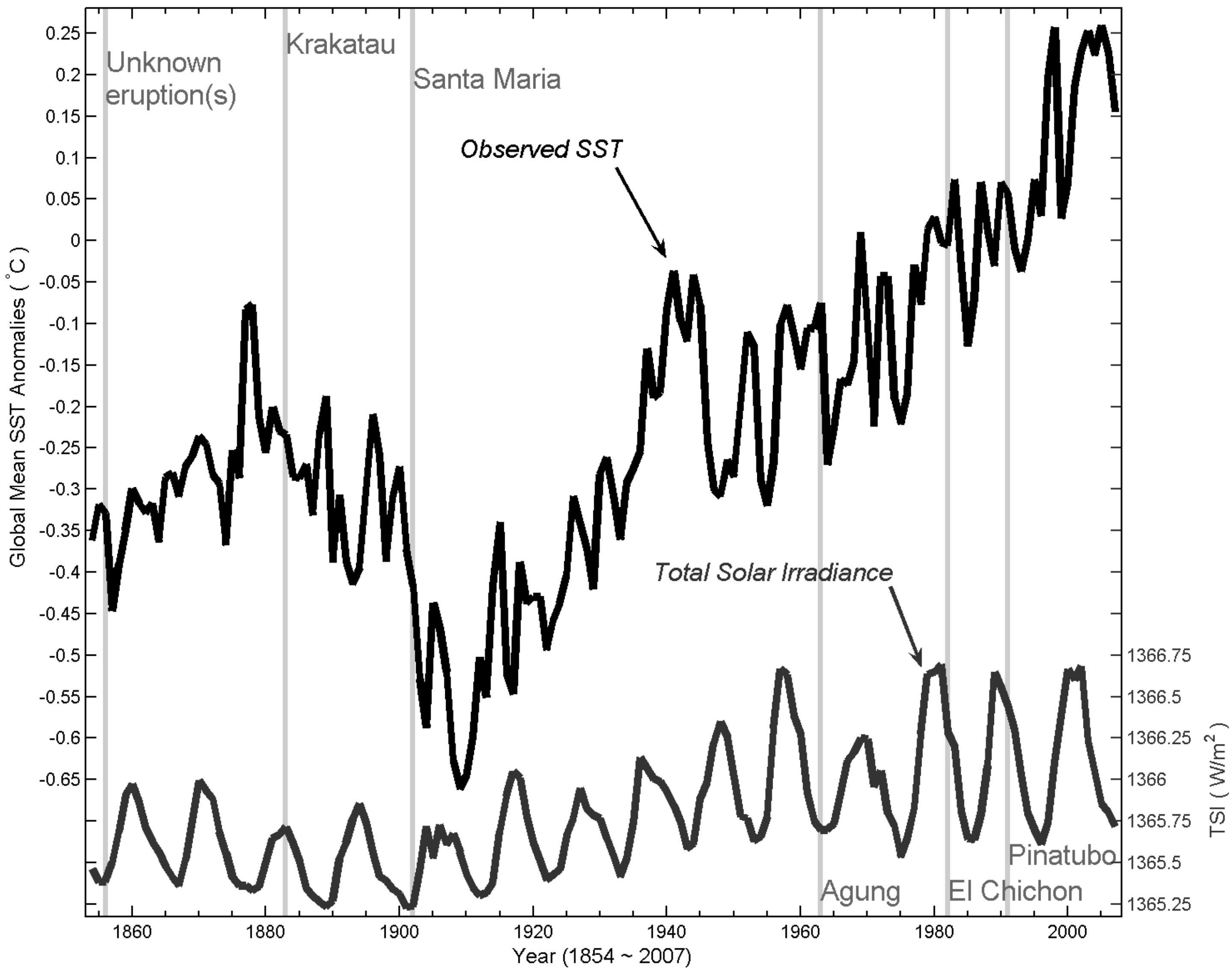

Figure 1. Sea-Surface Temperature, averaged from 60S-60N over the ocean areas, from NOAA's ERSST dataset from 1854-2008, top. Solar constant (Total Solar Irradiance) from Lean *et al.* [2005] and Wang *et al.* [2005] , bottom.

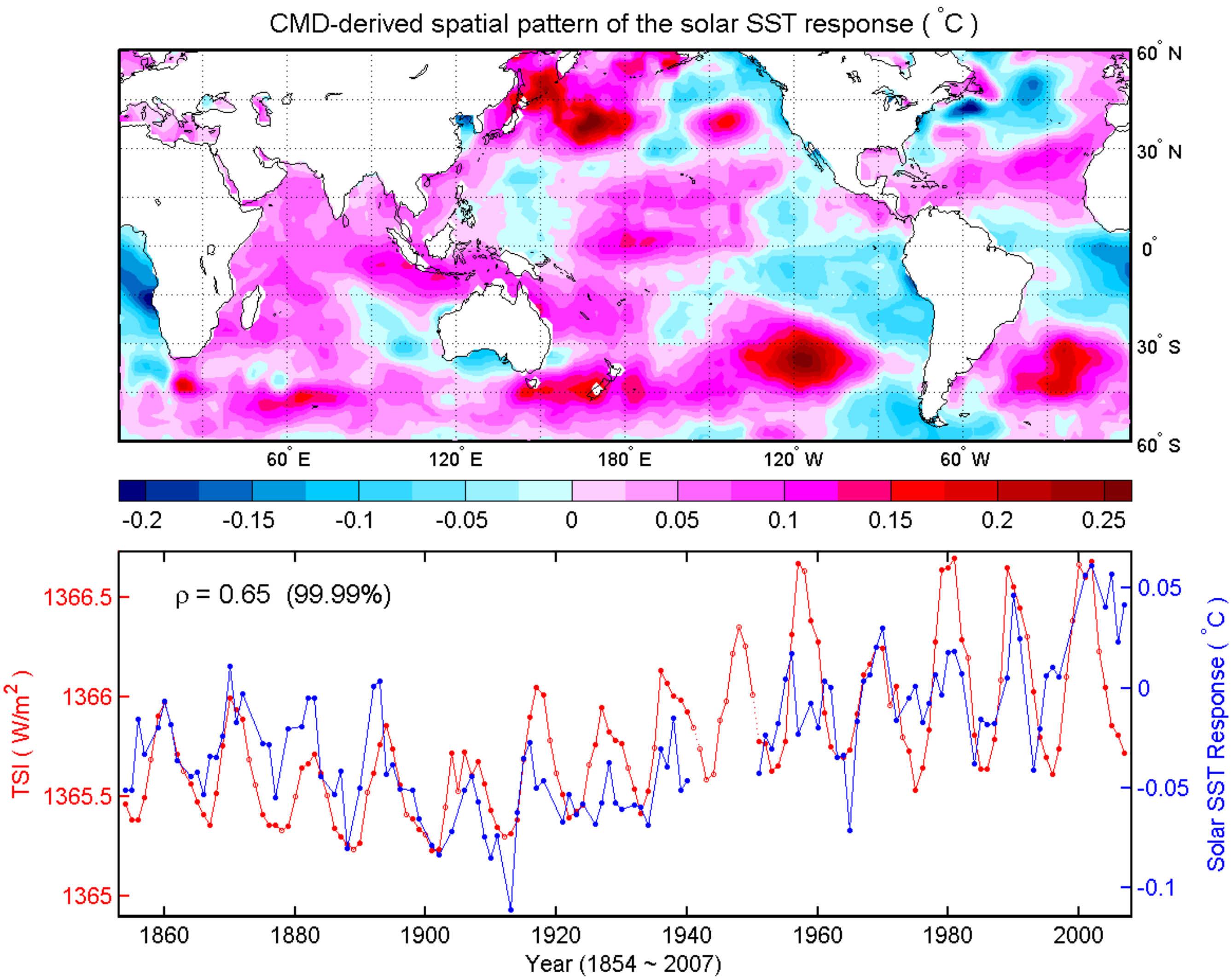

Figure 2. For the period 1854-2007, the spatial pattern of SST obtained from CMD in the top panel. The time series obtained by projecting the original data onto this pattern is shown in the lower panel in blue. The TSI index is shown in red. The correlation coefficient of the two curves is given by $\rho=0.65$, which is statistically significant at above 95% confidence level (99.99%) using bootstrap re-sampling with 10-year blocks of data.

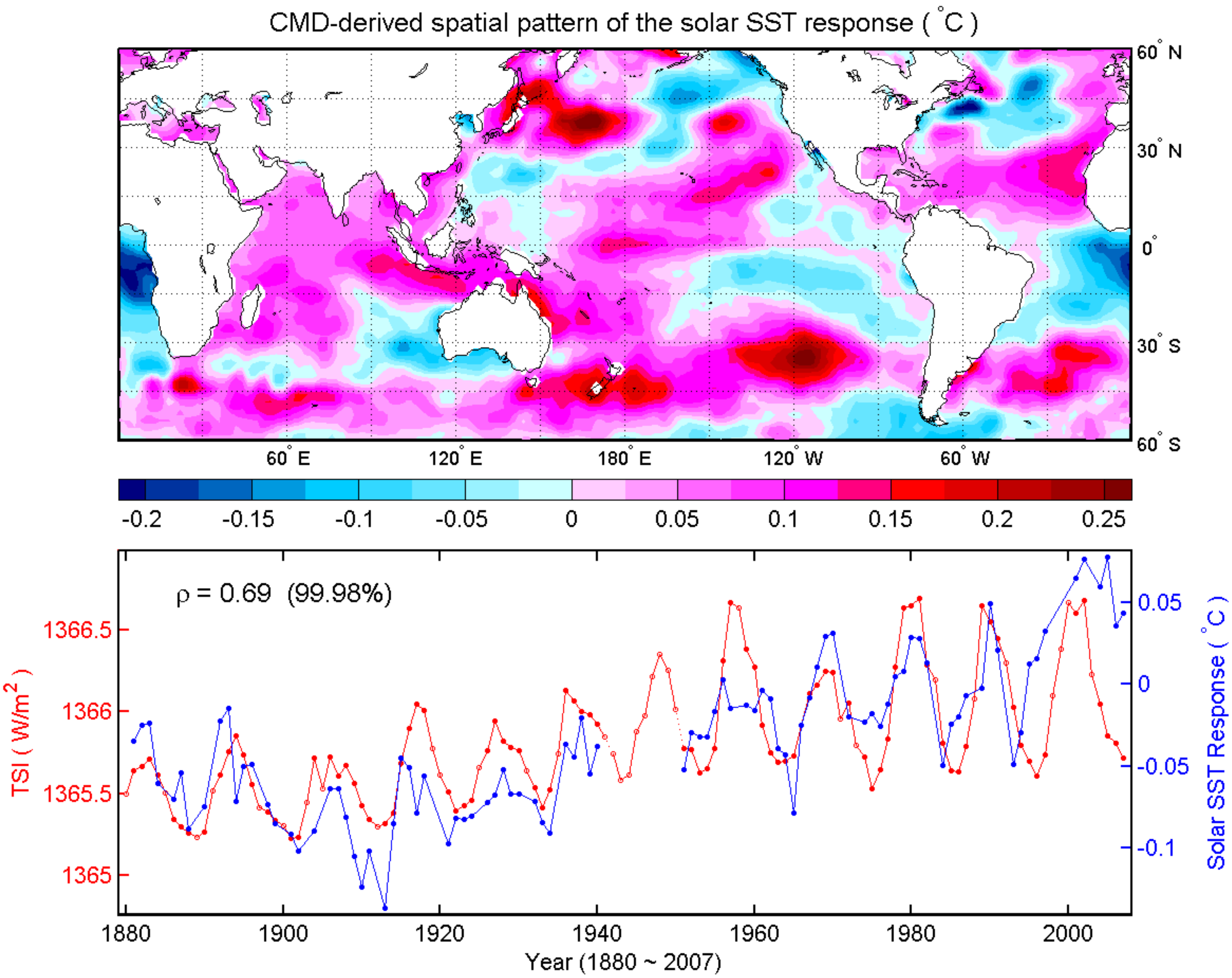

Figure 3. Same as Figure 2, except for the period 1880-2007.

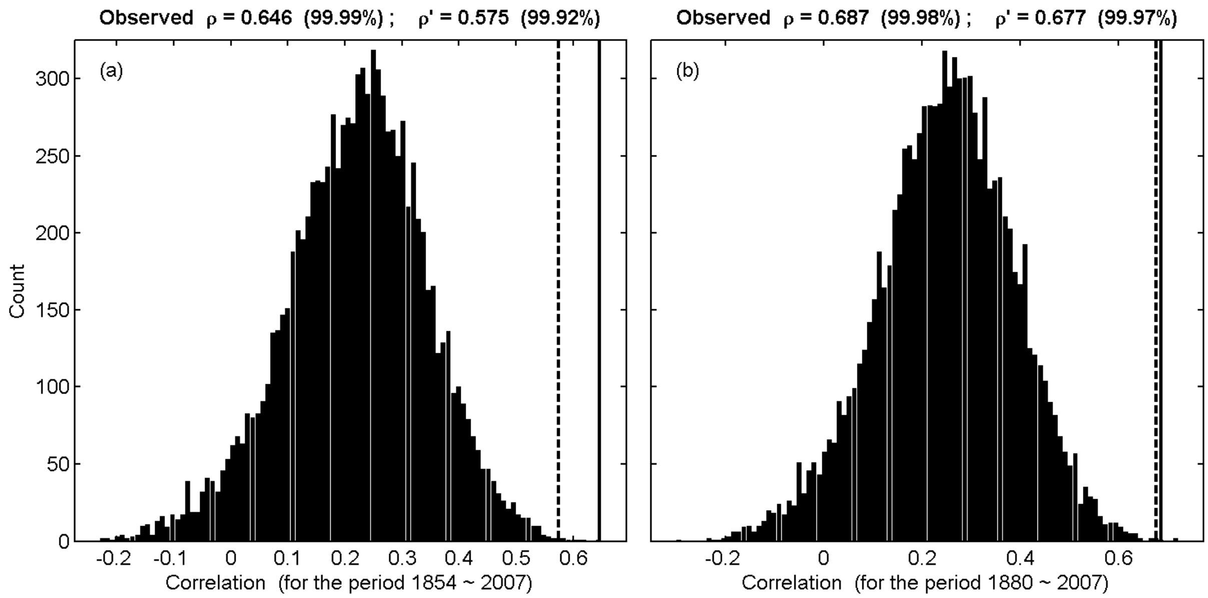

Figure 4. Distribution of the magnitude of correlation coefficients between the projected SST time series $C_1(t)$ and the solar TSI index, obtained using synthetic data generated by the *L*-block bootstrap re-sampling Monte-Carlo method. (a) For the period 1854-2007; (b) for the period 1880-2007. The solid vertical line is the observed ρ, and the dashed vertical line is the observed ρ obtained when the data was first detrended, denoted by ρ'. Note that here $C_1(t)$ is not normalized by the global mean of $P_1(\mathbf{x})$, which explains why the distribution is not bimodal.

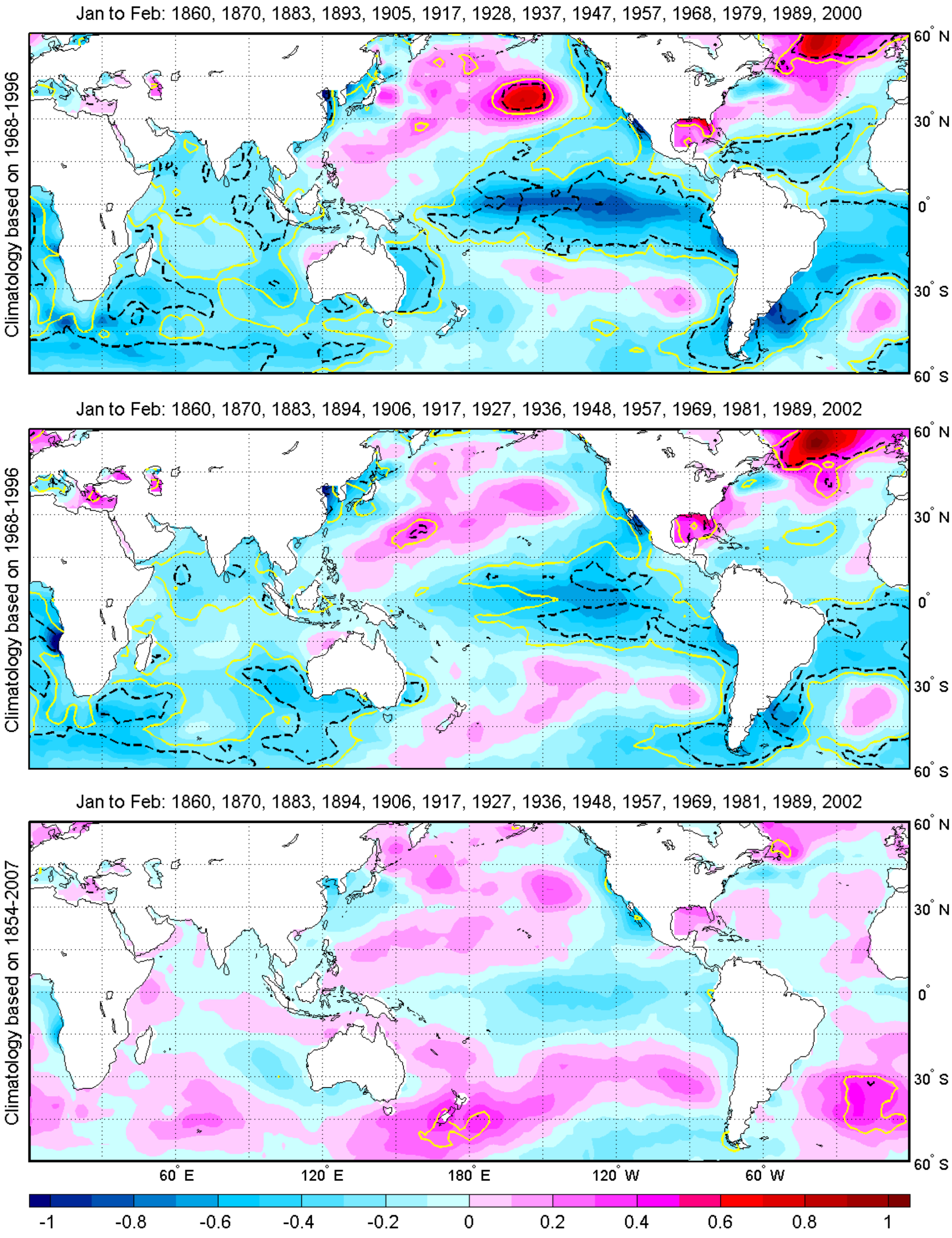

Figure 5. Difference in SST between the mean of the “solar peak years” (indicated at the top of the figure) during January to February over the period 1854-2007 and the “climatology” (computed for periods indicated along the left edge of the figure). Yellow contour enclose regions of 95% confidence level; dashed black contour encloses regions of 99% confidence level. Top panel: solar peak years determined by peaks in sunspot number; climatology determined by the period 1968-1996 chosen by Van Loon and Meehl [2008] . Middle panel: solar peak years

determined by peaks in TSI; climatology determined by the period 1968-1996; bottom panel: solar peak years determined by the peaks in TSI; climatology determined by the whole period of data record, 1854-2007.

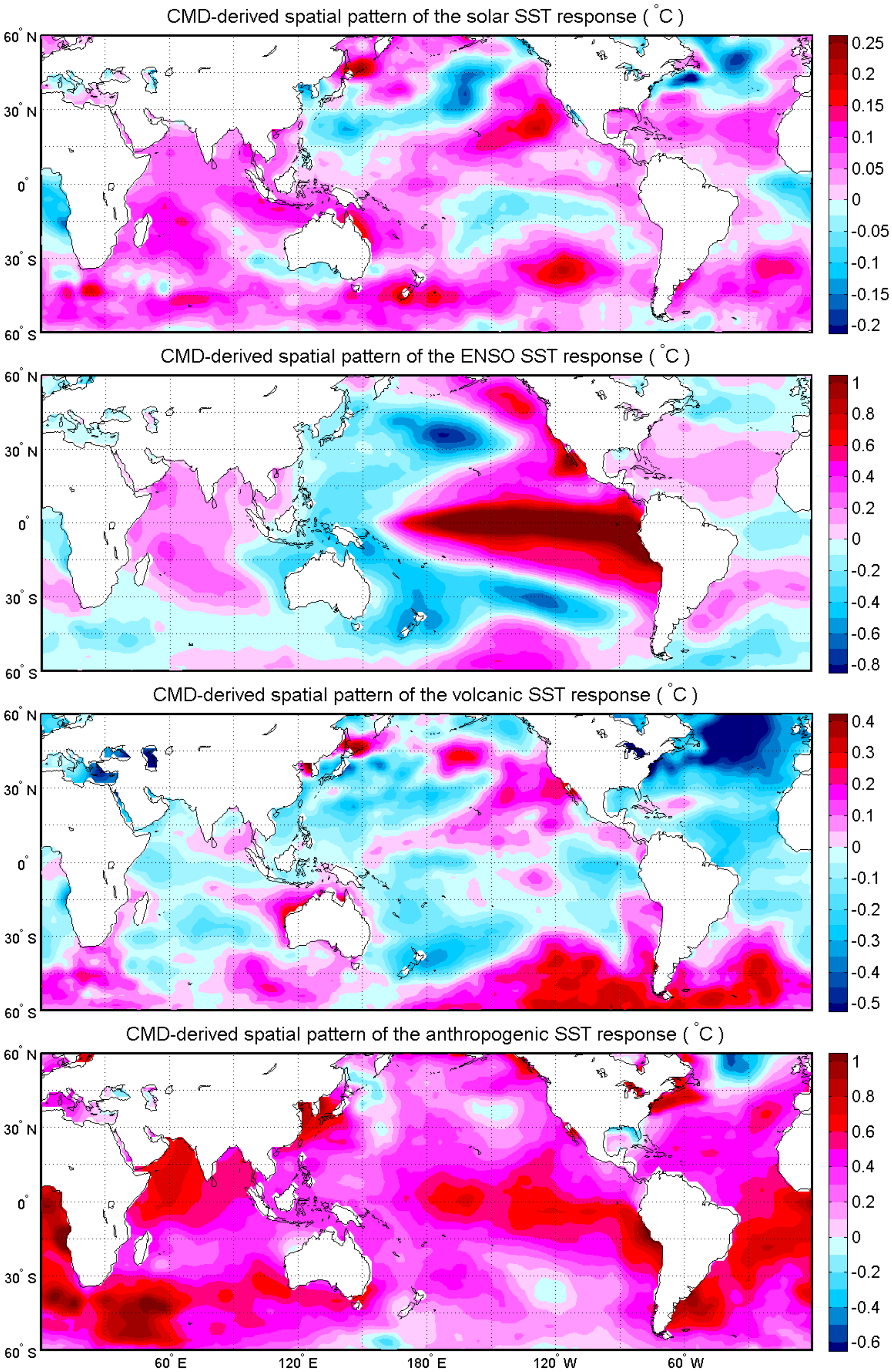

Figure 6: Spatial pattern in SST response derived using Multiple-CMD Inversion method for, from the top to bottom panels: solar cycle, ENSO, volcano aerosols, and greenhouse gas increases.